J Arid Land (2025) 17(2): 271–284
doi: 10.1007/s40333-025-0074-y; CSTR: 32276.14.JAL.0250074y

Science Press Springer-Verlag

Root system architecture and its scaling relationships of *Reaumuria soongorica* in Alxa steppe desert, Northwest China

MA Xiongzhong[1,2], WANG Xinping[3*], XIONG Weihong[1,2]

[1] School of Geographical Science and Planning, Nanning Normal University, Nanning 530001, China;
[2] Key Laboratory of Environment Change and Resources Use in Beibu Gulf, Ministry of Education, Nanning Normal University, Nanning 530001, China;
[3] Northwest Institute of Eco-Environment and Resources, Chinese Academy of Sciences, Lanzhou 730000, China

Abstract: Root system architecture has often been overlooked in plant research despite its critical role in plant adaptation to environmental conditions. This study focused on the root system architecture of the desert shrub *Reaumuria soongorica* in the Alxa steppe desert, Northwest China. Plant samples were collected during May–September 2019. Using excavation methods, *in situ* measurements, and root scanning techniques, we analyzed the root distribution, topology, and branching patterns of *R. soongorica* across an age sequence of 7–51 a. Additionally, we investigated the allometric relationships of root collar diameter with total coarse root length, biomass, and topological parameters. The results showed that the roots of *R. soongorica* were predominantly concentrated in shallow soil layers (10–50 cm), with lateral root branching and biomass allocation increasing with shrub age. The root topology exhibited a herringbone-like structure, with average topological and modified topological indices of 0.89 and 0.96, respectively, both of which adjusted with shrub age. The root system displayed a self-similar branching pattern, maintaining a constant cross-sectional area ratio of 1.13 before and after branching, deviating from the area-preserving rule. These adaptive traits allow *R. soongorica* to efficiently expand its nutrient acquisition zone, minimize internal competition, and optimize resource uptake from the upper soil layers. Furthermore, significant linear relationships were observed between $\log_{10}$-transformed root collar diameter and $\log_{10}$-transformed total coarse root length, biomass, and topological parameters. These findings advance non-destructive approaches for studying root characteristics and contribute to the development of root-related models. Besides, this study provides new insights into the adaptive strategies of *R. soongorica* under extreme drought conditions, offering valuable guidance for species selection and cultivation in desert restoration efforts.

Keywords: *Reaumuria soongorica*; root system architecture; root topology; root branching pattern; area-preserving rule; Alxa steppe desert

Citation: MA Xiongzhong, WANG Xinping, XIONG Weihong. 2025. Root system architecture and its scaling relationships of *Reaumuria soongorica* in Alxa steppe desert, Northwest China. Journal of Arid Land, 17(2): 271–284. https://doi.org/10.1007/s40333-025-0074-y; https://cstr.cn/32276.14.JAL.0250074y

1 Introduction

Roots are essential for the exchange of nutrients, water, and energy between plants and their soil environment (Omary et al., 2022). Root system architecture (RSA), defined as the spatial distribution and arrangement of roots within the soil, is critical for plant adaptation to

*Corresponding author: WANG Xinping (E-mail: xpwang@lzb.ac.cn)
Received 2024-07-23; revised 2024-12-20; accepted 2024-12-23

environmental conditions (Lynch, 2018). RSA demonstrates significant plasticity, varying both among species and within species across diverse habitats (Shan et al., 2018; Shelden and Munns, 2023). This plasticity has been harnessed in advanced breeding techniques to produce stress-tolerant plants that can maintain biomass stability under adverse environmental conditions (Ober et al., 2021; Ranjan et al., 2022). Additionally, adaptations in RSA provide insights for replanting strategies to combat soil degradation and support ecological succession (Karlova et al., 2021).

Research has shown that desert plants adapt to arid, nutrient-poor soils by altering aspects of RSA—including root distribution (Chen et al., 2023), topology (Kirschner et al., 2021), and morphology (Li et al., 2022a)—to enhance water and nutrient uptake (Fitter, 1987; Shelden and Munns, 2023). Kirschner et al. (2021) reviewed that some desert plants can survive by developing deep taproots to access groundwater, while others produce shallow roots and take advantage of short rainy seasons and irregular rainfall. Fitter (1987) identified two extreme root branching patterns: dichotomous and herringbone (Fig. 1). Dichotomous systems, characterized by dense secondary branches and high internal competition, cover a smaller area than herringbone systems given the same carbon investment, making them less effective for exploring nutrient-rich soil. In contrast, the herringbone pattern, with sparser branching, is better adapted for water and nutrient acquisition in arid, nutrient-limited environments (Magalhães and Seifert, 2015). Root branching strategies play a critical role in plant adaptation to various environments (Preti et al., 2022). Richter (1970) proposed that the cross-sectional area (CSA) of a tree trunk or branch is equal to the combined CSA of its higher-level branches, a concept known as the area-preserving rule. Numerous models of root growth and function have applied this rule (Magalhães and Seifert, 2015; Price et al., 2022), generally supporting its validity, though some exceptions exist (Salas-Alvarado et al., 2004). Desert plants thrive in arid environments and their root branching strategies are closely linked to the hydraulic structure of their root systems and other key adaptive mechanisms (Preti et al., 2022). However, our understanding of these strategies remains limited, including whether the root systems of typical desert species adhere to the area-preserving rule.

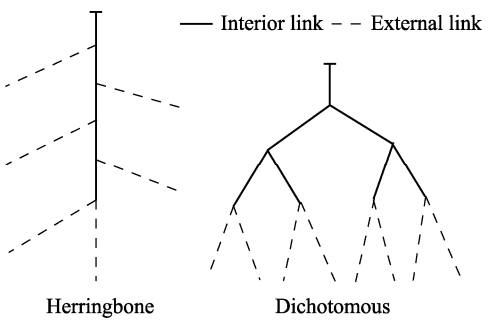

Fig. 1 Two extreme root branching patterns of herringbone and dichotomous (Fitter, 1987)

Due to the significant difficulty in excavating the root system of adult plants, most studies on RSA primarily focus on seedlings (Sorgonà et al., 2018; Li et al., 2022b), even though RSA is not constant throughout the plant life cycle (Oppelt et al., 2000). For example, Li et al. (2022b) studied the desert shrub *Nitraria tangutorum* in the West Ordos National Nature Reserve, China and demonstrated that as the shrub grew, root diameter (RD) increased, branching patterns became more intricate, and the range of nutrient utilization expanded. Bai et al. (2021) found that the root depth, branching number, specific root length, specific surface area, and RD of *Tamarix ramosissima* increased, while root branch angle and root-shoot ratio decreased with increasing shrub age in the oasis of Jinta County, Gansu Province, China. Understanding the dynamic changes in RSA—particularly in root distribution, topology, and branching patterns—across the life cycle of desert plants is essential for deciphering their drought adaptation strategies and for developing accurate root system models. In addition, some scaling relationships and allometries

of whole plants or plant organs have been extensively discussed in the literature (Ma and Wang, 2020; Wang et al., 2020). Understanding these scaling relationships for specific species is crucial for advancing non-destructive methods to investigate plant root characteristics.

Reaumuria soongorica is a small perennial shrub in the Tamaricaceae, widely distributed across the deserts of Central Asia and serving as one of the dominant species in the Alxa steppe desert of Northwest China. The belowground RSA of this shrub species provides critical insights into plant adaptive strategies under extreme drought conditions. We hypothesize that the RSA of *R. soongorica* (including root distribution, topology, and branching patterns) changes with shrub age to adapt to environmental stress, aiming to address three main questions: (1) how does the RSA of *R. soongorica* vary with age in an extremely arid habitat? (2) what branching strategies does *R. soongorica* employ to survive in such environments? and (3) how can key root system parameters be efficiently obtained through simple and measurable indicators?

2 Material and methods

2.1 Study area

The study area (37°25′N–42°47′N, 97°10′E–106°54′E; Fig. 2a) is located on the southwestern edge of the Alxa Plateau in Northwest China. The region experiences a typical continental arid climate, with mean annual temperature of 9.4°C and annual precipitation of 119.5 mm during 1999–2018 (Ma and Wang, 2020). The natural vegetation primarily comprises shrub species, including *R. soongarica*, *Salsola passerine*, *Nitraria sibirica*, *Sarcozygium xanthoxylon*, and *Kalidium foliatum*. Total vegetation coverage in the study area is 18.6%, with *R. soongarica* accounting for 61.8% of this coverage, making it the most widely distributed desert shrub in the region (Fig. 2b). The soil is classified as grey-brown desert soil, composed of 62.0% sand, 20.0% silt, and 18.0% clay (Fig. 2c). Groundwater levels are over 40 m below the surface, as determined by local well measurements, making precipitation the sole source of soil moisture replenishment.

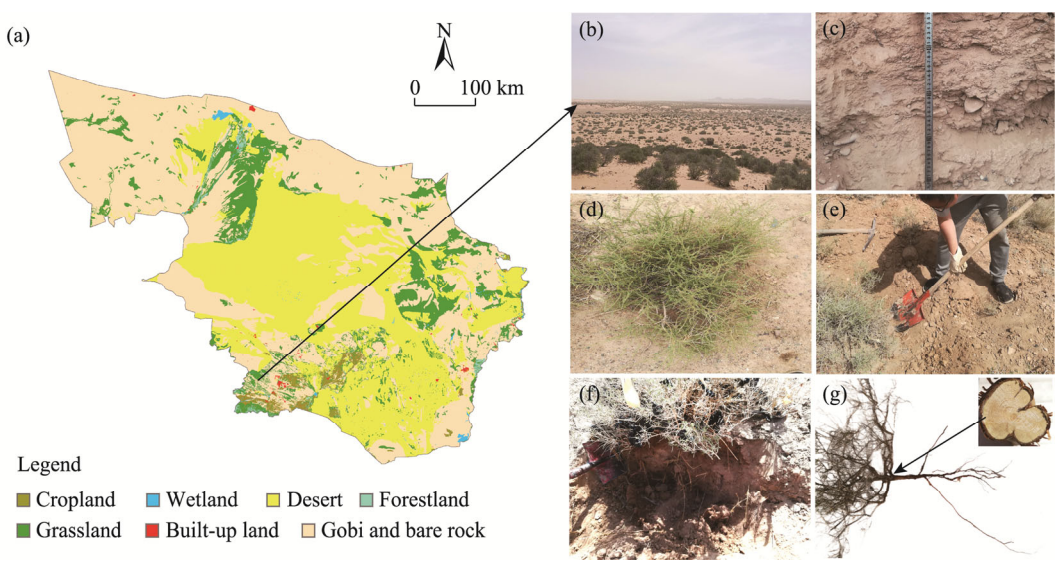

Fig. 2 Overview of the study area (a) and photos showing the landscape of the sampling plot (b), soil profile (c), dominant shrub species *Reaumuria soongorica* (d), field sampling of *R. soongorica* (e), root profile of *R. soongorica* (f), and ring and root system architecture of *R. soongorica* (g)

2.2 Data collection

From May to September in 2019, we selected a naturally flat area with uniform vegetation distribution and consistent soil nutrient and moisture levels as the sampling plot within the study

area to conduct the sample collection (Fig. 2b–e). The plot size was 500 m×500 m. A total of 66 *R. soongorica* shrubs with varying sizes were randomly selected, ensuring a minimum distance of 10 m between each shrub. The shrubs were cut at the base using pruning shears, and high-resolution images of their growth rings were captured to determine shrub age through ring counting (Fig. 2f and g; Ma and Wang, 2020). Because fine roots (diameter≤2.0 mm) have high turnover rates and are difficult to collect completely (Ma et al., 2021), only coarse roots (diameter>2.0 mm) were included in the topological modeling.

The coarse roots of each shrub were carefully excavated intact with a shovel by digging outward from the shrub base until the entire coarse root system was unearthed. The roots were then manually cleaned with a brush, transported to the laboratory, and mapped onto grid paper for precise measurements (Yang et al., 2008). For each shrub, we recorded the number of taproot nodes (N_{tn}), lateral roots per taproot node (N_{lr}), total number of nodes (N; including lateral root nodes), the number of external links (v_0) and interior links, total number of links (v; sum of interior and external links), and the maximal horizontal and vertical extensions of coarse roots (mm). External links refer to links at the terminal ends of the root system, reflecting the interconnected relationships among the plant root system, its surrounding environment, and other organisms. Interior links represent internal connections within the root system, facilitating the effective allocation of resources among different root parts (Fig. 3). The interior and external link lengths (mm) were measured using a measuring tape. The root collar diameters (RCD; mm) of each shrub and the RD before branching (d_0; mm) and after branching (d_j; mm) at each node were measured using an electronic digital caliper (Yang et al., 2008). The coarse roots were sorted into taproot and lateral roots, oven-dried at 65.0°C to a constant weight, cooled for 4–6 h, and weighed using an electronic balance (range: 0.01–500.00 g; resolution: 0.01 g) to determine the biomass of taproot (B_t; g) and lateral coarse roots (B_{lcr}; g) per shrub. A total of 66 *R. soongorica* shrubs were collected, ranging in age from 7 to 51 a. Based on age distribution, the shrubs were grouped into three age classes: 0–19 a (25 shrubs), 20–29 a (25 shrubs), and ≥30 a (16 shrubs) (Ma and Wang, 2020). Figure 3 gives the details of root branching patterns of *R. soongorica.*

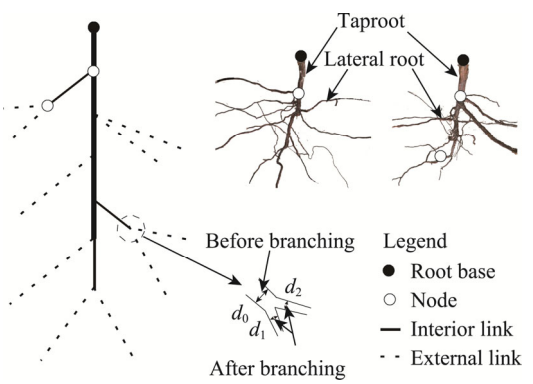

Fig. 3 Root branching patterns of *R. soongorica*. d_0 is the root diameter before root branching; d_1 and d_2 are the root diameters after branching.

2.3 Data processing and analysis

The data analysis workflow for this study is illustrated in Figure 4. Based on the node and link data, we calculated the topological parameters for each root system. Altitude (a) refers to the longest path (a path with the most links) from the root base to external links. The external path length (P_e) represents the sum of all path lengths from external links to the root base. Mean topological depth (b) is the average path length from external links to the root base and is calculated using the equation $b=P_e/v_0$. Mean external link length (l_e; mm) and mean interior link length (l_i; mm) refer to the average lengths of the external and interior links, respectively (Fitter, 1987; Oppelt et al., 2000; Shan et al., 2013; Magalhães et al., 2015).

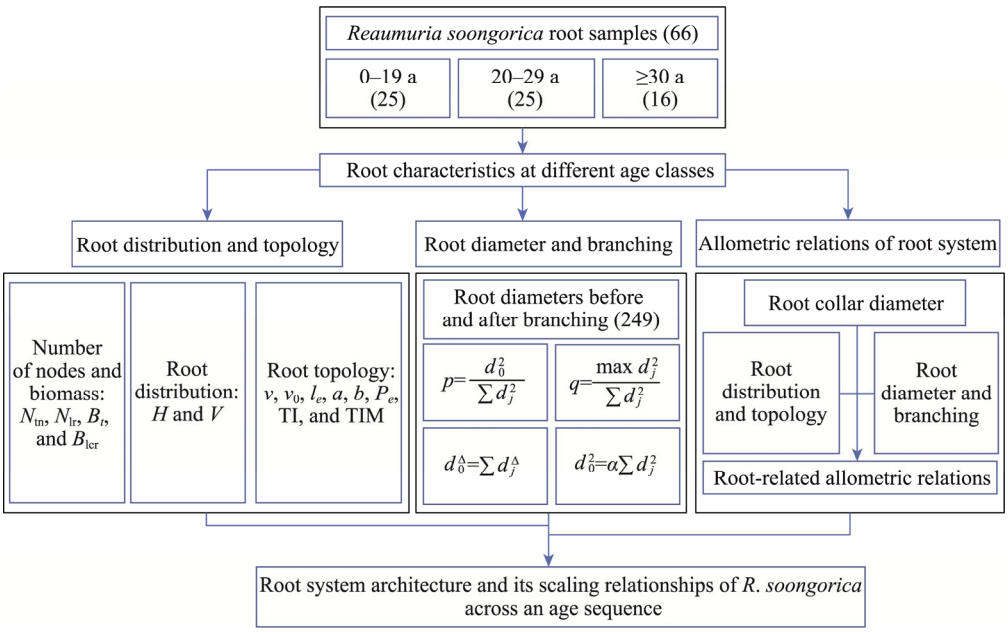

Fig. 4 Workflow of the data analysis in the present study. N_{tn} represents the number of taproot nodes per shrub; N_{lr} represents the number of lateral roots per taproot node; B_t represents the biomass of taproot per shrub; B_{lcr} represents the biomass of lateral coarse roots per shrub; H represents the root maximal horizontal extension; V represents the root maximal vertical extension; v represents the total number of links; v_0 represents the number of external links; l_e represents the mean external link length; l_i represents the mean interior link length; a represents the altitude, which is the longest path (a path with the most links) from the root base to external links; b represents the topological depth; P_e represents the external path length, which is the sum of all path lengths from external links to the root base; p represents the proportionality factor; d_j represents the root diameter after branching; q represents the allocation factor; Δ represents the diameter exponent; α represents the regression slope; TI represents the topological index; TIM represents the modified topological index. Values in parentheses represent the sample sizes.

The root topology of *R. soongorica* shrubs was estimated using the topological index (TI) and the modified topological index (TIM), and the formulas are as follows (Magalhães and Seifert, 2015):

$$\mathrm{TI} = \log_{10}(a) / \log_{10}(v_0)\,, \tag{1}$$

$$\mathrm{TIM} = \log_{10}(a) / \log_{10}(N+1)\,. \tag{2}$$

The TI values range from 0.53 to 1.00. When a TI value is closer to 1.00, it indicates a herringbone branching pattern, while a value closer to 0.53 suggests a dichotomous branching pattern (Fitter, 1987). TIM preserves the TI value when there is one lateral root per node and modifies it for cases with multiple branches per node. The range of TIM is the same as TI (Magalhães and Seifert, 2015).

The proportionality factor (p) was defined as the ratio of CSA before and after branching and was used to describe the change in CSA at branching points in both taproot and lateral root nodes (van Noordwijk and Mulia, 2002). The allocation factor (q) was defined as the ratio of the maximum CSA after branching to the total CSA after branching, which can describe the distribution equity of CSA after branching (van Noordwijk and Mulia, 2002; Magalhães and Seifert, 2015). The formulas are as follows:

$$p = \frac{d_0^2}{\sum d_j^2}\,, \tag{3}$$

$$q = \frac{\max(d_j^2)}{\sum d_j^2}\,. \tag{4}$$

The independence of p and q from shrub age and link diameter was tested by performing linear regressions between the branching parameters (p and q) and both shrub age and link diameter, and by testing the significance of the regression slopes. The self-similar branching pattern was confirmed when the branching parameters were not significantly different across age classes and did not depend on shrub age and link diameter (Magalhães and Seifert, 2015).

We analyzed the CSA before and after branching using the following three methods. First, the average p value was analyzed by t-test with the null hypothesis that p=1.00 for each age class and the entire age sequence. Second, the diameter exponent (Δ; a generalization of area-preserving rule) for each root node was estimated using Newton's method, and the average Δ values for each age class and the entire age sequence were computed. Third, a linear regression through the origin (Δ=2.00) of CSA before branching against CSA after branching was performed using Equation 6, another generalization of the area-preserving rule (Magalhães and Seifert, 2015). The average Δ and regression slope (α) for each age class and the entire age sequence were tested by t-test, with the null hypothesis that Δ=2.00 and α=1.00. If the average p, Δ, or α values did not reject the null hypothesis, the area-preserving rule was confirmed. If p>1.00, Δ<2.00, or α>1.00, the CSA after branching was less than that before branching; if p<1.00, Δ>2.00, or α<1.00, the result was the opposite (Oppelt et al., 2000; Magalhães and Seifert, 2015). The formulas are as follows:

$$d_0^{\Delta} = \sum d_j^{\Delta} \quad , \tag{5}$$

$$d_0^2 = \alpha \sum d_j^2 \quad . \tag{6}$$

Scaling relationships between RCD (mm) and total coarse root length (L_{cr}; mm), total coarse root biomass (B_{cr}; g), and topological parameters (v, v_0, a, b, and P_e), as well as between RD (mm) of a specific root segment and its total distal length (the length of all links behind this root segment) (L_d; mm) were analyzed using a logarithmically transformed univariate allometric function:

$$\ln(y) = \ln f + c \ln(x) , \tag{7}$$

where y is the RSA parameter (e.g., L_{cr}, B_{cr}, v, v_0, a, b, P_e, and L_d); x is the RCD or RD; and f and c are the allometric coefficients.

This study conducted Analysis of Variance (ANOVA) and Least Significant Difference (LSD) tests to assess differences in root distribution, topological parameters, branching parameters, as well as the exponent Δ across age classes. Pearson's correlation matrix was used to analyze relationships between shrub age, root distribution, and topological parameters. All the statistical analyses were performed at the 0.05 significance level using Microsoft Excel Data Analysis Tools and SPSS 18.0 (SPSS Inc., Chicago, IL, USA).

3 Results

3.1 Root distribution and topology of *R. soongorica*

The roots of *R. soongorica* were predominantly concentrated in the 10–50 cm soil layer, characterized by a prominent taproot with minimal branching (Figs. 2g and 3). At older age class, lateral roots extended more horizontally, while the taproot remained the primary and thickest root axis. N_{tn}, N_{lr}, and the proportion of taproot nodes with multiple lateral roots all increased significantly with age (Table 1; Fig. 5). At all age classes, B_t accounted for more than half of the B_{cr}, and the proportion of B_{lcr} relative to the B_{cr} also increased with age (Table 1; Fig. 5).

The v and v_0 increased significantly with age (Fig. 5; Table 2). The l_e showed no significant variation across age classes, while l_i decreased with age. At all age classes and throughout the entire sequence, l_i was consistently shorter than l_e. Maximal horizontal and vertical extensions, a, b, and P_e all increased with age. Both TI and TIM values decreased significantly with age. For TI, the null hypotheses equal to 1.00 or 0.53 were rejected across all age classes and the pooled data (P<0.05). For TIM, these hypotheses were rejected at the two older age classes and across the entire age sequence, but not at the younger age class 0–19 a (P=0.06).

Table 1 Summary of the root distribution parameters for *Reaumuria soongorica* at each age class

Parameter	Age class			
	0–19 a	20–29 a	≥30 a	Mean
Number of taproot nodes per shrub (N_{tn})	2.9±0.3^{a}	3.8±0.4^{ab}	4.6±0.4^{b}	3.6±0.2
Number of lateral roots per taproot node (N_{lr})	1.2±0.1^{a}	1.2±0.1^{a}	1.4±0.1^{b}	1.3±0.0
Proportion of taproot nodes with one lateral root (%)	83.3	79.8	67.6	77.0
Proportion of taproot nodes with multiple lateral roots (%)	16.7	20.2	32.4	23.0
Biomass of taproot per shrub (B_t; g)	17.1±2.8^{a}	24.7±3.1^{ab}	28.6±3.1^{b}	22.7±1.8
Biomass of lateral coarse roots per shrub (B_{lcr}; g)	10.2±2.2^{a}	17.2±2.4^{ab}	25.7±5.0^{b}	16.6±1.9

Note: Values are mean±SE. The sample sizes were 25, 25, and 16 for age classes of 0–19, 20–29, and ≥30 a, respectively. Significant differences among different columns are indicated by distinct lowercase letters (P<0.05).

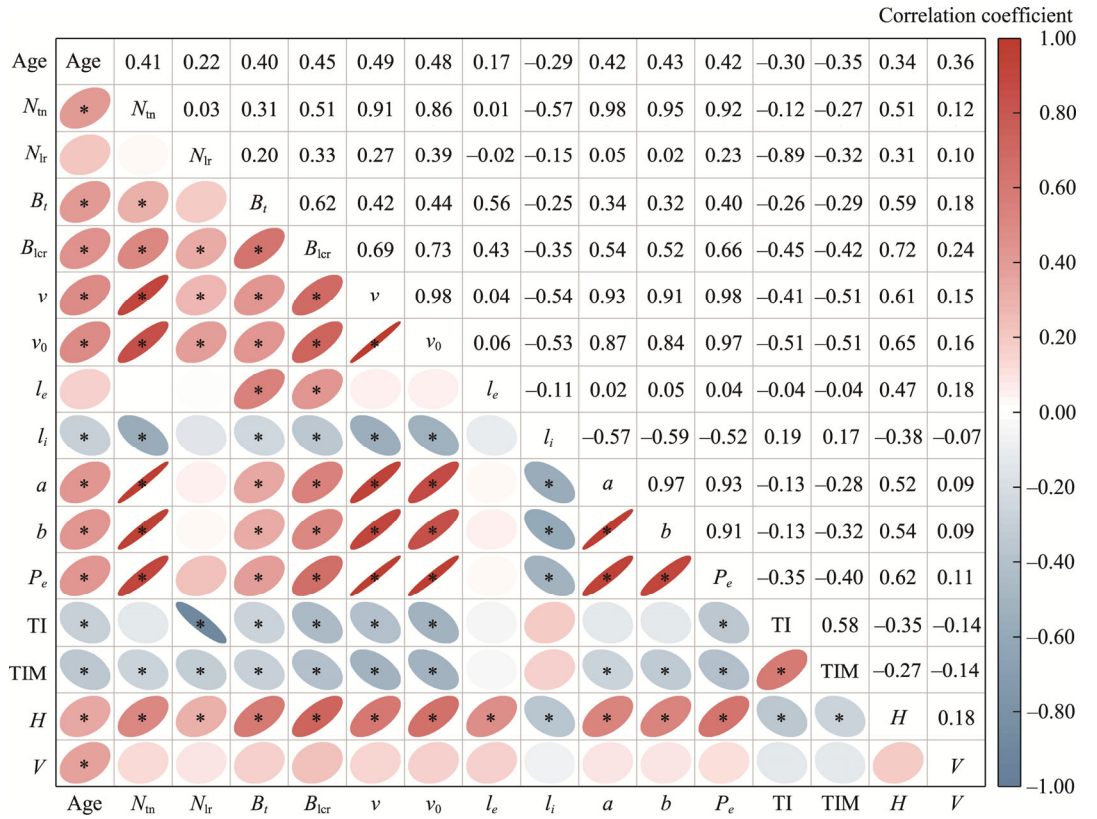

Fig. 5 Correlation analysis between root distribution and topological parameters. * indicates a significant correlation at the P<0.05 level.

3.2 Root branching of *R. soongorica*

The average branching parameter p ranged from 1.09 to 1.20 across the three age classes, with an overall average of 1.13 (Table 3). Values for each age class and the entire age sequence differed significantly from the null hypothesis of p=1.00, with no significant differences among different age classes. The average q value per node showed an overall average of 0.75 across all age classes, showing no significant differences among different age classes.

Linear regressions of p with shrub age (Adjusted R^2=0.006 and P=0.12) and link diameter (Adjusted R^2=0.005 and P=0.13) were not significant (Table 3; Fig. 6). The independence of q values from shrub age (Adjusted R^2= –0.004 and P=0.91) and link diameter (Adjusted R^2= –0.004 and P=0.91) was also confirmed for all root nodes (Adjusted R^2= –0.002 and P=0.43) (Table 3; Fig. 6).

Table 2 Topological parameters of the root systems for *R. soongorica* at each age class

Parameter	Age class			
	0–19 a	20–29 a	≥30 a	Mean
Number of links (v)	7.7±0.8[a]	10.6±1.1[b]	14.6±1.1[c]	10.5±0.7
Number of external links (v_0)	4.6±0.5[a]	6.2±0.6[a]	8.8±0.7[b]	6.2±0.4
Mean external link length (l_e; mm)	357.9±42.2[a]	372.5±32.3[a]	374.4±37.2[a]	367.4±22.2
Mean interior link length (l_i; mm)	98.0±14.7[a]	82.1±9.1[ab]	62.4±6.2[b]	83.4±6.8
Maximal horizontal extension (mm)	313.2±28.1[a]	346.5±22.2[ab]	412.3±26.8[b]	350.7±15.4
Maximal vertical extension (mm)	346.4±18.3[a]	404.8±19.5[b]	425.6±13.5[b]	387.4±11.7
Altitude (a)	3.9±0.3[a]	5.0±0.4[b]	5.7±0.3[b]	4.7±0.2
Mean topological depth (b)	3.2±0.2[a]	3.7±0.2[b]	4.1±0.1[b]	3.6±0.1
External path length (P_e)	16.7±2.7[a]	25.9±4.2[a]	37.3±3.9[b]	25.2±2.3
Topological index (TI)	0.92±0.02[a]	0.90±0.02[a]	0.81±0.03[b]	0.89±0.01
Modified topological index (TIM)	0.98±0.01[a]	0.96±0.01[a]	0.91±0.02[b]	0.96±0.01

Note: Values are mean±SE. The sample sizes were 25, 25, and 16 for age classes of 0–19, 20–29, and ≥30 a, respectively. Significant differences among different columns are indicated by distinct lowercase letters (P<0.05).

Table 3 Summary of basic statistics for the branching parameters and the diameter exponent (Δ)

Parameter	Statistical indicator	Age class			
		0–19 a	20–29 a	≥30 a	All ages
p	Minimum	0.65	0.38	0.57	0.38
	Maximum	1.95	2.74	3.75	3.75
	Mean	1.10[a]	1.09[a]	1.20[a]	1.13
	Standard error	0.03	0.03	0.05	0.02
	P-value	0.00	0.00	0.00	0.00
q	Minimum	0.37	0.36	0.43	0.36
	Maximum	0.98	0.98	0.98	0.98
	Mean	0.75a	0.74a	0.75a	0.75
	Standard error	0.02	0.02	0.02	0.01
	P-value	0.00	0.00	0.00	0.00
Δ	Minimum	1.00	0.81	0.86	0.81
	Maximum	4.84	5.61	3.57	5.61
	Mean	1.88[ab]	1.95[a]	1.71[b]	1.85
	Standard error	0.08	0.10	0.06	0.05
	P-value	0.15	0.62	0.00	0.00

Note: p represents the proportionality factor; q represents the allocation factor; P-value represents the probability that the observed results are consistent with the null hypothesis of p=1.00, q=0.50, and Δ=2.00 at different age classes. The sample sizes were 70, 101, and 78 for age classes of 0–19, 20–29, and ≥30 a, respectively. Significant differences are denoted by distinct lowercase letters (P<0.05).

The average Δ values across the three age classes ranged from 1.71 to 1.95, with an overall overage of 1.85 (Table 3). For age classes 0–19 and 20–29 a, the null hypothesis of Δ=2.00 was not rejected (P>0.05). However, for the age class ≥30 a and the entire age sequence, the average Δ values were significantly lower than 2.00 (Table 3).

A significant positive linear relationship was observed between CSA before and after branching across all age classes and the entire age sequence (Fig. 7). The slope α differed significantly from 1.00 at all age classes, except for the age class ≥30 a (Fig. 7).

3.3 Root-related allometric relationships of *R. soongorica*

The $\log_{10}$-transformed RCD exhibited a strong linear relationship with $\log_{10}$-transformed L_{cr} in the pooled data, with a slope of 1.77 (P<0.05; Fig. 8a). The scatter plot of $\log_{10}$-transformed RD and L_d showed a wider scattering (Adjusted R^2=0.578 and P<0.05) than that of $\log_{10}$-transformed

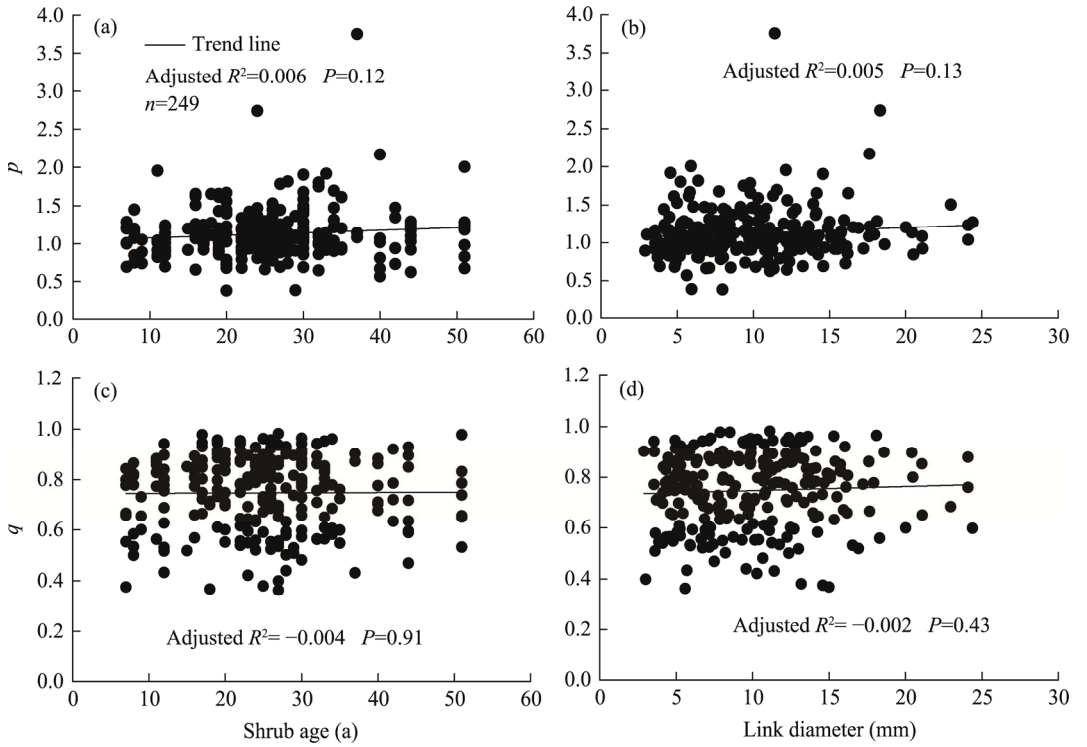

Fig. 6 Regression of root branching parameters (p and q) against shrub age (a and c) and link diameter (b and d)

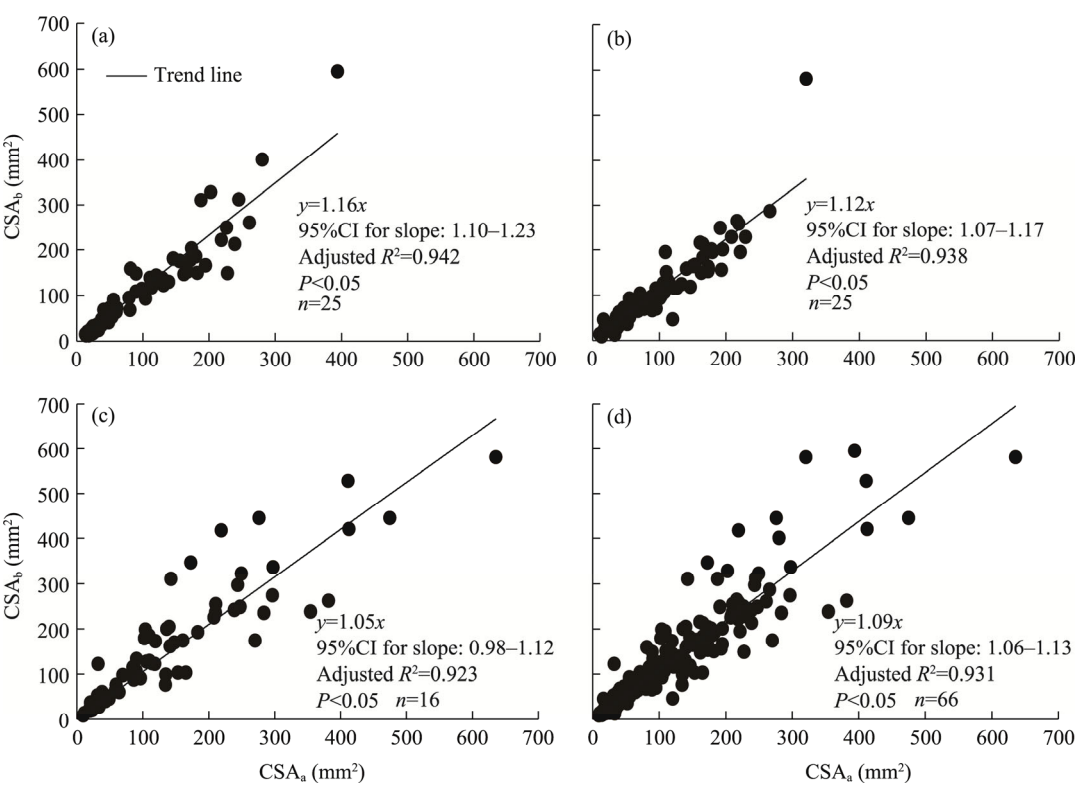

Fig. 7 Linear regression (through the origin) of cross-sectional area before branching (CSA_b) against cross-sectional area after branching (CSA_a) for age classes of 0–19 a (a), 20–29 a (b), and ≥30 a (c), and the entire age sequence (d). 95%CI represents the 95% confidence interval.

RCD and L_{cr} (Fig. 8b). The $\log_{10}$-transformed RCD exhibited a consistent relationship with $\log_{10}$-transformed B_{cr}, with a regression slope of 2.31 (Adjusted R^2=0.892 and P<0.05) across all age classes (Fig. 8c).

The regression between $\log_{10}$-transformed RCD and v yielded a slope of 1.51, with an intercept of –0.88 and an Adjusted R^2 of 0.733. The regression between $\log_{10}$-transformed RCD and v_0 yielded a slope of 1.27, with an intercept of –0.80 and an Adjusted R^2 of 0.742. The regression between $\log_{10}$-transformed RCD and a had a slope of 1.01, an intercept of –0.58, and an adjusted R^2 of 0.668. The regression between $\log_{10}$-transformed RCD and b showed a slope of 0.78, with an intercept of 0.08 and an Adjusted R^2 of 0.662. The regression between $\log_{10}$-transformed RCD and P_e yielded a slope of 2.05, with an intercept of –1.21 and an Adjusted R^2 of 0.718 (Table 4).

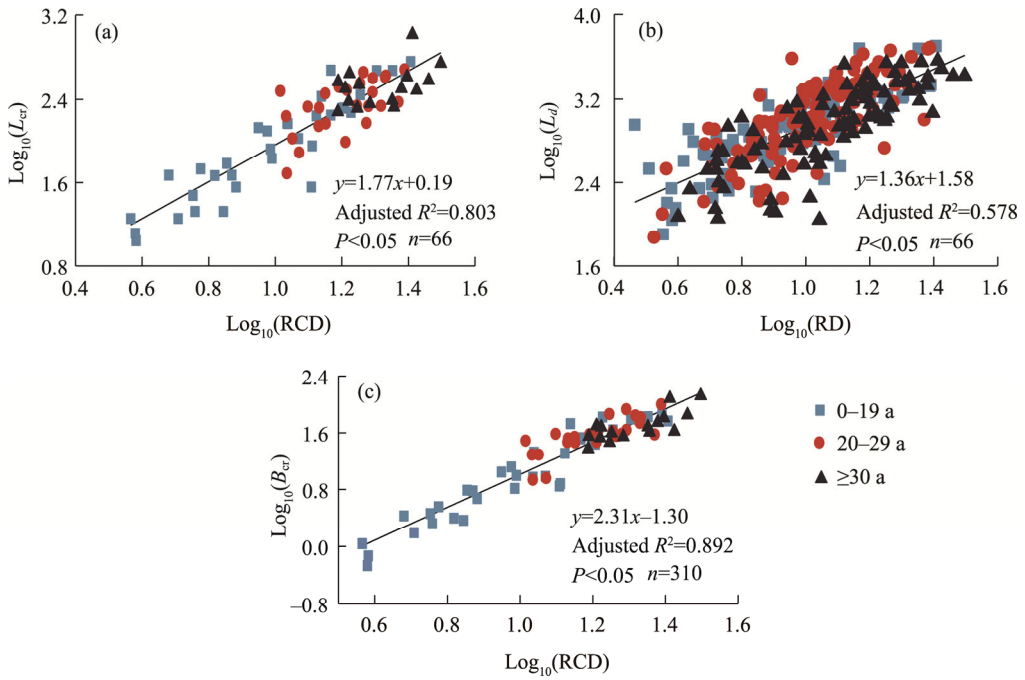

Fig. 8 Scaling relationships in the root systems of *R. soongorica*. (a), relationship between $\log_{10}$-transformed root collar diameter (RCD) and total coarse root length (L_{cr}); (b), relationship between $\log_{10}$-transformed root diameter (RD) and total distal length (L_d); (c), relationship between $\log_{10}$-transformed RCD and total coarse root biomass (B_{cr}).

Table 4 Linear regression of $\log_{10}$-transformed root collar diameter (RCD) and topological parameters (v, v_0, a, b, and P_e)

Scaling relationship	Slope	95%CI	Intercept	Adjusted R^2	P-value
Between $\log_{10}$(RCD) and $\log_{10}(v)$	1.51	1.30–1.72	–0.88	0.733	<0.05
Between $\log_{10}$(RCD) and $\log_{10}(v_0)$	1.27	1.09–1.44	–0.80	0.742	<0.05
Between $\log_{10}$(RCD) and $\log_{10}(a)$	1.01	0.84–1.17	–0.58	0.668	<0.05
Between $\log_{10}$(RCD) and $\log_{10}(b)$	0.78	0.65–0.91	0.08	0.662	<0.05
Between $\log_{10}$(RCD) and $\log_{10}(P_e)$	2.05	1.76–2.35	–1.21	0.718	<0.05

Note: 95%CI represents the 95% confidence interval. The sample size for each scaling relationship was 66.

4 Discussion

4.1 Root topology and its adaptive strategy

In this study, the maximal vertical extension of coarse roots for *R. soongorica* increased with age,

but averaged only 387.4 mm, which is shallower than previously reported for this species in the Hexi Corridor, Northwest China (Shan et al., 2018). This relatively shallow root system is likely a response to the extreme drought conditions in the study area, where groundwater is deep, and soil moisture is primarily replenished through precipitation and condensation (Pan et al., 2018; Ma and Wang, 2020). Furthermore, since nutrients are concentrated in the topsoil in this region (Ma et al., 2024), horizontal root growth may be more advantageous than deep vertical growth for accessing both water and nutrients. Indeed, we observed a significant positive correlation between shrub age and maximal horizontal extension of coarse roots. This finding aligns with previous studies (Lynch, 2013; Uga et al., 2013; Karlova et al., 2021), which suggested that drought conditions promote more economical root systems, encouraging root elongation toward areas with higher water availability.

The average N_{lr}, the proportion of nodes with multiple lateral roots, and the biomass ratio of lateral roots all increased with age, further supporting the idea that *R. soongorica* shrubs primarily develop lateral roots with age to enhance nutrient acquisition. This pattern aligns with the benefit-cost theory, which suggested that plants allocate more carbon to root components that improve nutrient uptake (Preti et al., 2022). Similarly, studies by Dhief et al. (2011) and He et al. (2016) and have shown that under water stress, plants increase lateral root length and biomass to expand their horizontal range and reduce root competition. The l_e values did not differ significantly across age classes, likely due to the increased branching of lateral roots, with many external links arising from lateral root branches rather than directly from the taproot (Fig. 3). Overall, the increased lateral root branching and biomass allocation, along with the expansion of the root foraging range, may represent an adaptive strategy for shrubs in arid environments.

The average TI and TIM values for *R. soongarica* were 0.89 and 0.96, respectively, indicating a branching pattern resembling a herringbone structure, consistent with the findings on desert plants by Yang et al. (2008) and Li et al. (2015). According to Fitter (1987), herringbone root systems, characterized by fewer branches and longer root extension, are advantageous in environments with limited water or nutrients. This trait aligns with the root characteristics of *R. soongarica* (Shan et al., 2013; Ma and Wang, 2020) and may be an adaptation to the resource scarcity in this region (Magalhães and Seifert, 2015). In this study, the topological indices TI and TIM of *R. soongarica* decreased with age, suggesting that the species adjusts its root topology as it matures. These findings are in agreement with the study results of Oppelt et al. (2000), who observed a similar decrease in four plant species in Botswana. Overall, root topology may be influenced by both environmental conditions and self-regulation, particularly in arid areas, making *R. soongorica* a useful indicator of shrub adaptive strategies.

4.2 Root branching characteristics

The average p and q did not differ significantly across age classes and the entire age sequence, confirming their independence from both shrub age and link diameter (Table 3). This suggested a self-similar branching pattern in the root systems. The constant CSA rule likely contributes to a uniform hydraulic architecture across the root systems, enhancing water transport efficiency, reducing hydraulic resistance, and ensuring consistent distribution of water and nutrients throughout the root systems (Preti et al., 2022). Similar patterns have been observed in other common shrub species in the steppe desert of North China, including *N. tangutorum*, *Tamarix chinensis*, *Periploca sepium*, and *Calligonum roborovskii* (Yang et al., 2008; Shan et al., 2013; Zhao et al., 2015).

The area-preserving rule did not apply to the root systems of *R. soongarica*, as all three methods consistently showed a reduction in CSA after branching compared to that before branching. This reduction in CSA may be attributed to lateral root embolism (Nikolova et al., 2009; Bucci et al., 2013). Under drought conditions, terminal roots often experience embolism and die off, reducing CSA towards the root tips. This could help isolate parts of the plant from the effects of the arid soil layer (Bucci et al., 2013). Another possible explanation for the decrease is the higher proportion of

inactive heartwood in thicker roots, which reduces the CSA available for water and nutrient transport, thus increasing the CSA ratio before and after branching (Anfodillo et al., 2006; Magalhães and Seifert, 2015). Similar findings were reported in the study of *N. tangutorum* in the central Hexi Corridor (Shan et al., 2013).

4.3 Allometric relationships of the root systems

The $\log_{10}$-transformed L_{cr}, B_{cr}, and topological parameters of *R. soongorica* showed strong correlations with $\log_{10}$-transformed RCD, consistent with previous studies (Oppelt et al., 2000; Yang et al., 2008). An allometric relationship between $\log_{10}$-transformed B_{cr} and RCD was reported by van Noordwijk et al. (1994) and Oppelt et al. (2000). Similarly, Yang et al. (2008) demonstrated that root configuration parameters in species such as *Tamarix taklamakanensis*, *C. roborovskii*, and *Apocynum venetum* could be predicted by RCD. This correlation likely results from the self-similar branching pattern of the root systems (Oppelt et al., 2000). Our results confirmed that both the CSA ratio before and after branching and the ratio of maximum to total CSA after branching remained consistent across age classes and the entire age sequence. Thus, the constant CSA rule may enable accurate estimations of coarse root parameters. Based on these scaling relationships, RCD could serve as a predictor for the RSA of *R. soongorica*, offering an effective means of indirectly assessing the spatial distribution of roots in the soil and their nutrient absorption efficiency.

5 Conclusions

This study revealed key characteristics of the RSA of *R. soongorica* shrubs in the Alxa steppe desert. The results showed that *R. soongorica* primarily developed lateral roots in shallow soil layers as the shrub ages, an adaptive trait that enhances its ability to expand nutrient acquisition and efficiently capture rainwater, condensation, and nutrients from the upper soil layers. The root topology followed a herringbone-like structure, which minimizes overlap and reduces nutrient competition. A consistent reduction in root CSA after branching was observed across various age classes and root segment diameters. This stable branching pattern enables accurate estimates of L_{cr}, B_{cr}, and topological parameters through allometric equations. Our findings enhance the understanding of the RSA of *R. soongorica* and offer practical insights for estimating root parameters, with implications for vegetation restoration and management in arid areas.

Conflict of interest

The authors declare that they have no known competing financial interests or personal relationships that could have appeared to influence the work reported in this paper.

Acknowledgements

This work was funded by the Guangxi Science and Technology Plan Project (Guike AD22080050), the Basic Research Ability Improvement Project of Young and Middle-aged Teachers of Universities in Guangxi (2022KY0386), the Opening Foundation of Key Laboratory of Environment Change and Resources Use in Beibu Gulf, Ministry of Education, Nanning Normal University (NNNU-KLOP-K2202), and the National Natural Science Foundation of China (42471055). The authors would like to thank the editors and the reviewers for their valuable comments that significantly improved the content and clarity of the article.

Author contributions

Conceptualization: WANG Xinping, MA Xiongzhong; Methodology: MA Xiongzhong, XIONG Weihong; Formal analysis: MA Xiongzhong, XIONG Weihong; Writing - original draft preparation: MA Xiongzhong; Writing - review and editing: MA Xiongzhong, WANG Xinping, XIONG Weihong; Funding acquisition: MA Xiongzhong; Supervision: WANG Xinping. All authors approved the manuscript.

References

Anfodillo T, Carraro V, Carrer M, et al. 2006. Convergent tapering of xylem conduits in different woody species. New Phytologist, 169(2): 279–290.

Bai X, Zhao C Z, Kang M P. 2021. Relationship between root forks and branch angle of *Tamarix ramosissima* at different stand ages in oasis of Jinta County. Acta Ecologica Sinica, 41(5): 1878–1884. (in Chinese)

Bucci S J, Scholz F G, Peschiutta M L, et al. 2013. The stem xylem of Patagonian shrubs operates far from the point of catastrophic dysfunction and is additionally protected from drought-induced embolism by leaves and roots. Plant, Cell & Environment, 36(12): 2163–2174.

Chen X Y, Chen Y J, Zhang W, et al. 2023. Response characteristics of root to moisture change at seedling stage of *Kengyilia hirsuta*. Frontiers in Plant Science, 13: 1052791, doi: 10.3389/fpls.2022.1052791.

Dhief A, Abdellaoui R, Tarhouni M, et al. 2011. Root and aboveground growth of rhizotron-grown seedlings of three Tunisian desert *Calligonum* species under water deficit. Canadian Journal of Soil Science, 91(1): 15–27.

Fitter A H. 1987. An architectural approach to the comparative ecology of plant root system. New Phytologist, 106(S1): 61–77.

He G Z, Chen Y N, Chen Y P, et al. 2016. Adaptive strategy of *Tamarix spp* root architecture in arid environment. Journal of Beijing Normal University (Natural Science), 52(3): 277–282. (in Chinese)

Karlova R, Boer D, Hayes S, et al. 2021. Root plasticity under abiotic stress. Plant Physiology, 187(3): 1057–1070.

Kirschner G K, Xiao T T, Blilou I. 2021. Rooting in the desert: A developmental overview on desert plants. Genes, 12(5): 709, doi: 10.3390/genes12050709.

Li C J, Guo J H, Zeng F J, et al. 2015. Shoot and root architectural variance and adaptability of *Tamarix ramosissima* in different ages. Journal of Desert Research, 35(2): 365–372. (in Chinese)

Li C J, Han H, Ablimiti M, et al. 2022a. Morphological and physiological responses of desert plants to drought stress in a man-made landscape of the Taklimakan desert shelter belt. Ecological Indicators, 140: 109037, doi: 10.1016/j.ecolind.2022.109037.

Li X L, Dang X H, Gao Y, et al. 2022b. Response mechanisms of adventitious root architectural characteristics of *Nitraria tangutorum* shrubs to soil nutrients in Nabkha. Plants, 11(23): 3218, doi: 10.3390/plants11233218.

Lynch J P. 2013. Steep, cheap and deep: an ideotype to optimize water and N acquisition by maize root systems. Annals of Botany, 112(2): 347–357.

Lynch J P. 2018. Rightsizing root phenotypes for drought resistance. Journal of Experimental Botany, 69(13): 3279–3292.

Ma X Z, Wang X P. 2020. Biomass partitioning and allometric relations of the *Reaumuria soongorica* shrub in Alxa steppe desert in NW China. Forest Ecology and Management, 468: 118178, doi: 10.1016/j.foreco.2020.118178.

Ma X Z, Wang X P, Jin Y X, et al. 2021. Fine root production, turnover of *Reaumuria songarica* and soil carbon and nitrogen in Alxa steppe desert of NW China. Restoration Ecology, 29(6): e13362, doi: 10.1111/rec.13362.

Ma X Z, Wang X P, Xiong W H. 2024. Fine-root turnover and leaf litterfall of *Salsola passerina* facilitate soil restoration in Alxa steppe desert of northwest China. Restoration Ecology, 32(6): e14040, doi: 10.1111/rec.14040.

Magalhães T M, Seifert T. 2015. Below- and aboveground architecture of *Androstachys johnsonii* prain: topological analysis of the root and shoot systems. Plant and Soil, 394(1): 257–269.

Nikolova P S, Blaschke H, Matyssek R, et al. 2009. Combined application of computer tomography and light microscopy for analysis of conductive xylem area in coarse roots of European beech and Norway spruce. European Journal of Forest Research, 128: 145–153.

Ober E S, Alahmad S, Cockram J, et al. 2021. Wheat root systems as a breeding target for climate resilience. Theoretical and Applied Genetics, 134(6): 1645–1662.

Omary M, Gil-Yarom N, Chen Y, et al. 2022. A conserved superlocus regulates above- and belowground root initiation. Science, 375(6584): eabf4368, doi: 10.1126/science.abf4368.

Oppelt A L, Kurth W, Dzierzon H, et al. 2000. Structure and fractal dimensions of root systems of four co–occurring fruit tree species from Botswana. Annals of Forest Science, 57(5–6): 463–475.

Pan Y X, Wang X P, Zhang Y F, et al. 2018. Dew formation characteristics at annual and daily scale in xerophyte shrub plantations at Southeast margin of Tengger desert, Northern China. Ecohydrology, 11(5): e1968, doi: 10.1002/eco.1968.

Preti F, Dani A, Noto L V, et al. 2022. On the Leonardo's rule for the assessment of root profile. Ecological Engineering, 179: 106620, doi: 10.1016/j.ecoleng.2022.106620.

Price C A, Drake P, Veneklaas E J, et al. 2022. Flow similarity, stochastic branching, and quarter–power scaling in plants. Plant Physiology, 190(3): 1854–1865.

Ranjan A, Sinha R, Singla-Pareek S L, et al. 2022. Shaping the root system architecture in plants for adaptation to drought stress. Physiologia Plantarum, 174(2): e13651, doi: 10.1111/ppl.13651.

Richter J P. 1970. The Notebooks of Leonardo Da Vinci. New York: Dover.

Salas E, Ozier-Lafontaine H, Nygren P. 2004. A fractal root model applied for estimating the root biomass and architecture in two tropical legume tree species. Annals of Forest Science, 61(4): 337–345.

Shan L S, Li Y, Ren W, et al. 2013. Root architecture of two desert plants in central Hexi Corridor of Northwest China. Chinese Journal of Applied Ecology, 24(1): 25–31. (in Chinese)

Shan L S, Su M, Zhang Z Z, et al. 2018. Vertical distribution pattern of mixed root systems of desert plants *Reaumuria soongarica* and *Salsola passerina* under different environmental gradients. Chinese Journal of Plant Ecology, 42(4): 475–486. (in Chinese)

Shelden M C, Munns R. 2023. Crop root system plasticity for improved yields in saline soils. Frontiers in Plant Science, 14: 1120583, doi: 10.3389/fpls.2023.1120583.

Sorgonà A, Proto A R, Abenavoli L M, et al. 2018. Spatial distribution of coarse root biomass and carbon in a high–density olive orchard: Effects of mechanical harvesting methods. Trees, 32: 919–931.

Uga Y, Sugimoto K, Ogawa S, et al. 2013. Control of root system architecture by *DEEPER ROOTING 1* increases rice yield under drought conditions. Nature Genetics, 45(9): 1097–1102.

van Noordwijk M, Spek L Y, de Willigen P. 1994. Proximal root diameter as predictor of total root size for fractal branching models: I. Theory. Plant and Soil, 164: 107–117.

van Noordwijk M, Mulia R. 2002. Functional branch analysis as tool for fractal scaling above- and belowground trees for their additive and non–additive properties. Ecological Modelling, 149(1–2): 41–51.

Wang G, Laga H, Jia J Y, et al. 2020. Statistical analysis and modeling of the geometry and topology of plant roots. Journal of Theoretical Biology, 486: 110108, doi: 10.1016/j.jtbi.2019.110108.

Yang X L, Zhang X M, Li Y L, et al. 2008. Analysis of root architecture and root adaptive strategy in the Taklimakan desert area of China. Chinese Journal of Plant Ecology, 32(6): 1268–1276. (in Chinese)

Zhao Y Y, Lu Z H, Xia J B, et al. 2015. Root architecture and adaptive strategy of 3 shrubs in Shell Bay in Yellow River Delta. Acta Ecologica Sinica, 35(6): 1688–1695. (in Chinese)